Supporting Information for

Enhancing the reversible capacity and cycling stability of sodium cathode materials by Li^+ reversible migration

Xingyu Li[abc], Ruguang Ma[d], Yang Gan[be], Yi Li[be], Wujie Qiu[*bc], Jifen Wang[*a] and Jianjun Liu[*bef]

[a.]School of Resources and Environmental Engineering, Shanghai Polytechnic University, Shanghai Engineering Research Center of Advanced Thermal Functional Materials, No.2360 Jinhai Rd., Shanghai 201209, China.

[b.]State Key Laboratory of High Performance Ceramics and Superfine Microstructure, Shanghai Institute of Ceramics, Chinese Academy of Sciences, 1295 Dingxi Road, Shanghai 200050, China.

[c.]School of Mathematics, Physics and Statistics, Shanghai Polytechnic University, No.2360 Jinhai Rd., Shanghai 201209, China.

[d.]School of Materials Science and Engineering, Suzhou University of Science and Technology, 99 Xuefu Road Suzhou, 215011, China.

[e.]Center of Materials Science and Optoelectronics Engineering, University of Chinese Academy of Sciences, Beijing 100049, China

[f.]School of Chemistry and Materials Science, Hangzhou Institute for Advanced Study, University of Chinese Academy of Science, 1 Sub-lane Xiangshan, Hangzhou, 310024, China.

*Email: jliu@mail.sic.ac.cn; wangjifen@sspu.edu.cn; wjqiu@sspu.edu.cn.

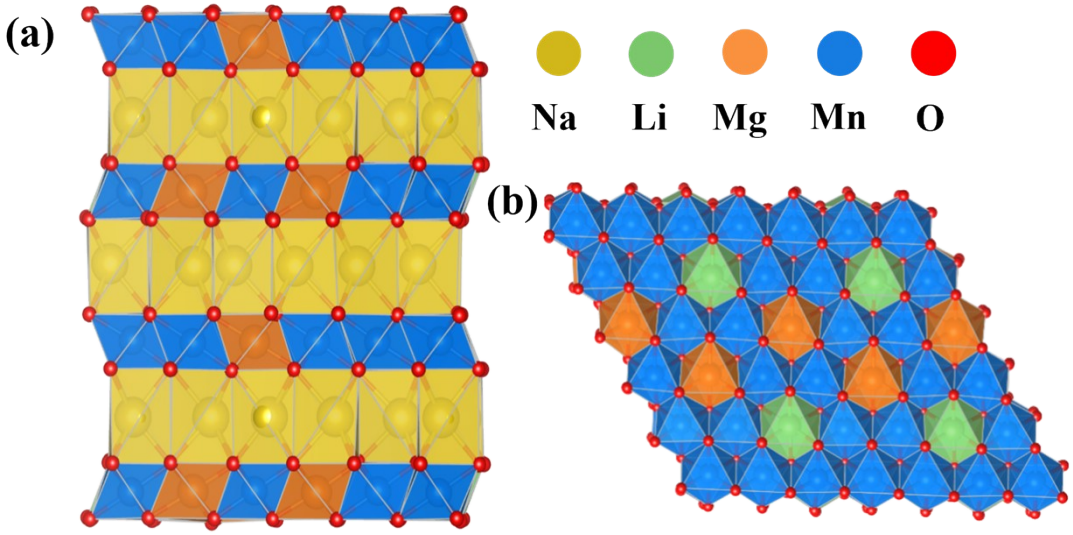

Figure S1. The cell structure model of NLMMO for DFT calculation. (a) The structure diagram obtained along the a-axis. (b) The structure diagram obtained along the c-axis.

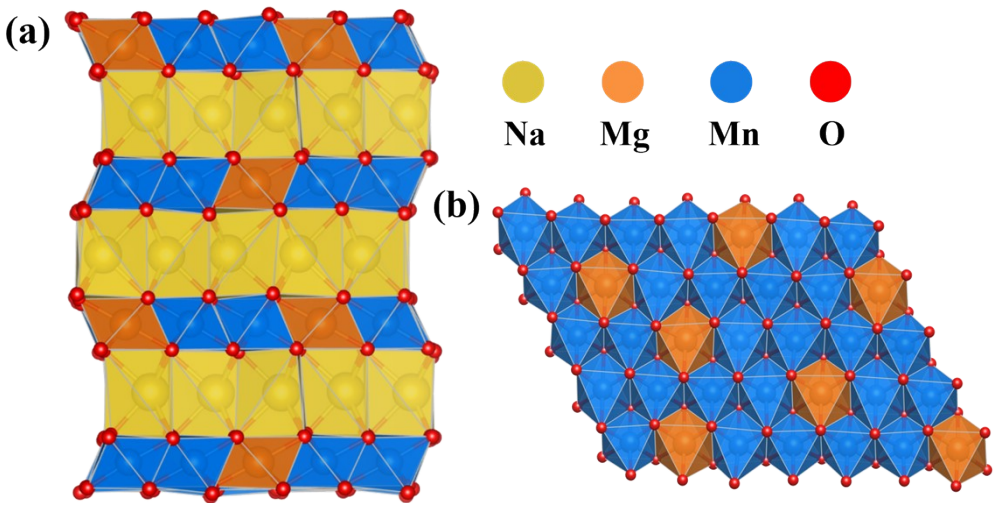

Figure S2. The cell structure model of NMMO for DFT calculation. (a) The structure diagram obtained along the a-axis. (b) The structure diagram obtained along the c-axis.

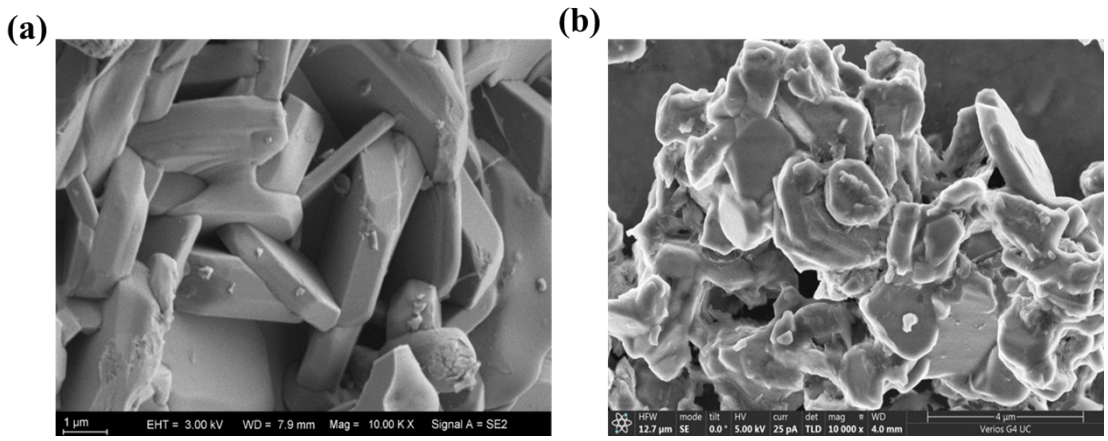

Figure S3. SEM images of (a) P2-NLMMO and (b) P2-NMMO. The surface of NLMMO is relatively smooth, while the surface of NMMO will have particles attached to it.

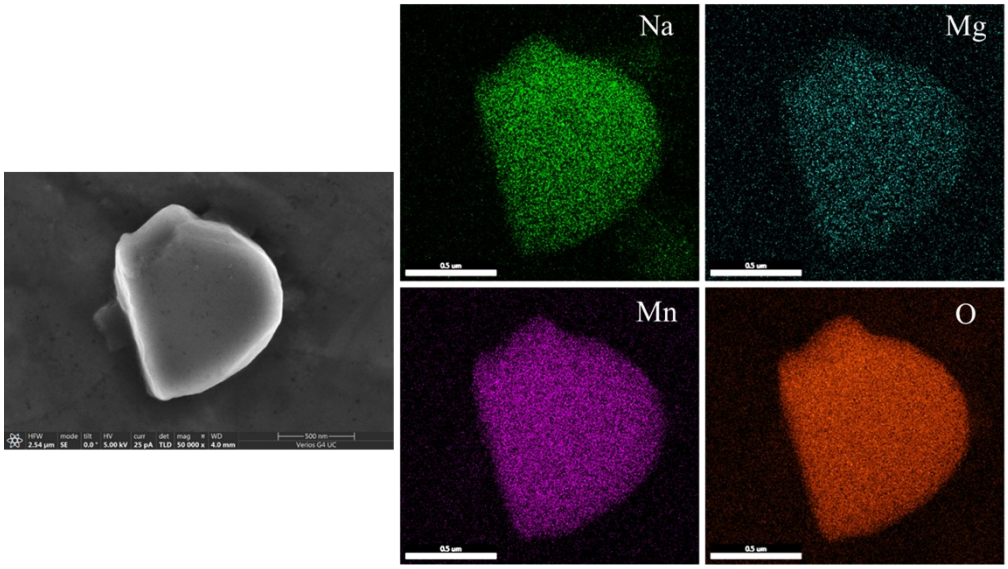

Figure S4. SEM image of P2-NMMO and the corresponding EDS mappings. The Na, Mg, Mn and O elements are uniformly distributed in the sample.

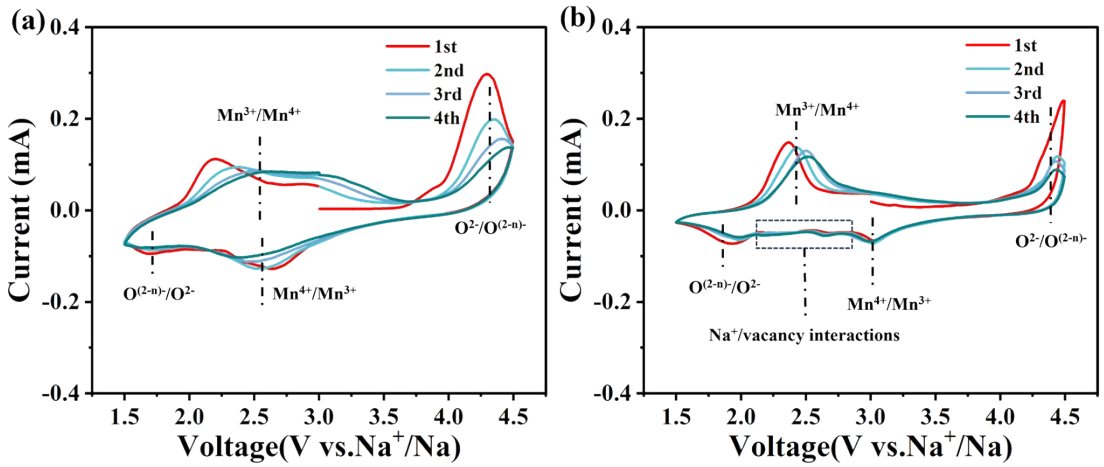

Figure S5. CV curves of (a) NLMMO and (b) NMMOat a scan rate of 0.1mV s^{-1}**.** The CV CURVES of NLMMO and NMMO all reflected the redox reactions of Mn^{3+}/Mn^{4+} and $O^{2-}/O^{(2-n)-}$. In addition, NMMO had the presence of Na^{+}/vacancy interactions.

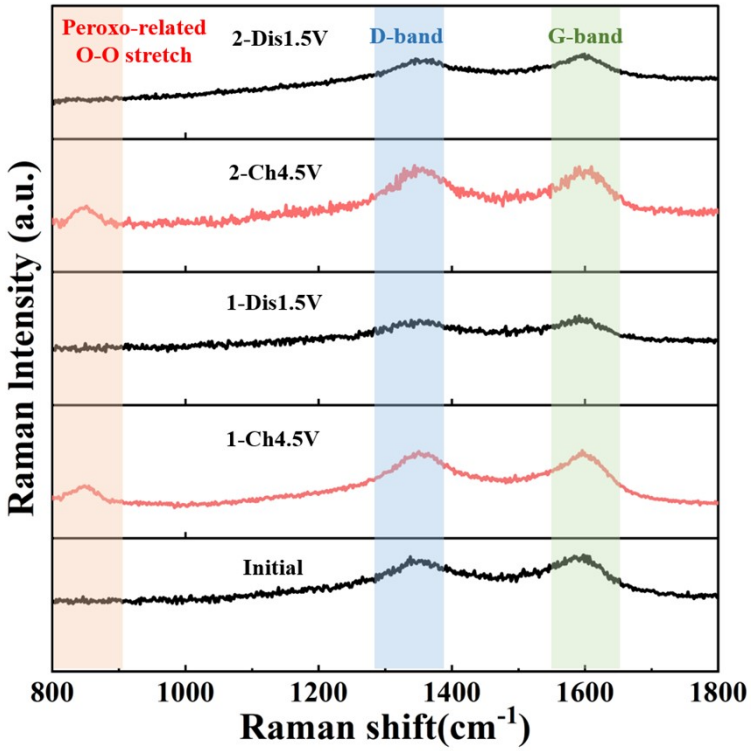

Figure S6. The *ex-situ* Raman spectra of NLMMO in the first two cycles. When charged to 4.5 V, the appearance of a new peak at 850 cm^{-1} represents the oxidation of O species. In the first two cycles, the change of peaks in the peroxo-related O-O stretching region demonstrated the redox activity of oxygen.

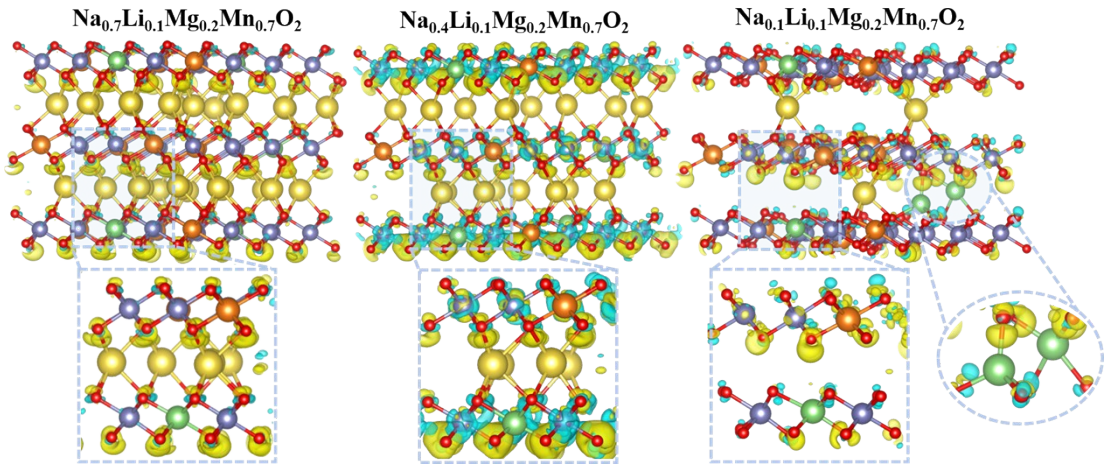

Figure S7. A plot of the charge density difference uopn desodiation. The yellow portion indicates an increase in charge density and the blue portion indicates a decrease in charge density. In the desodiation process, the increased charge density of oxygen indicates the oxidation of oxygen.

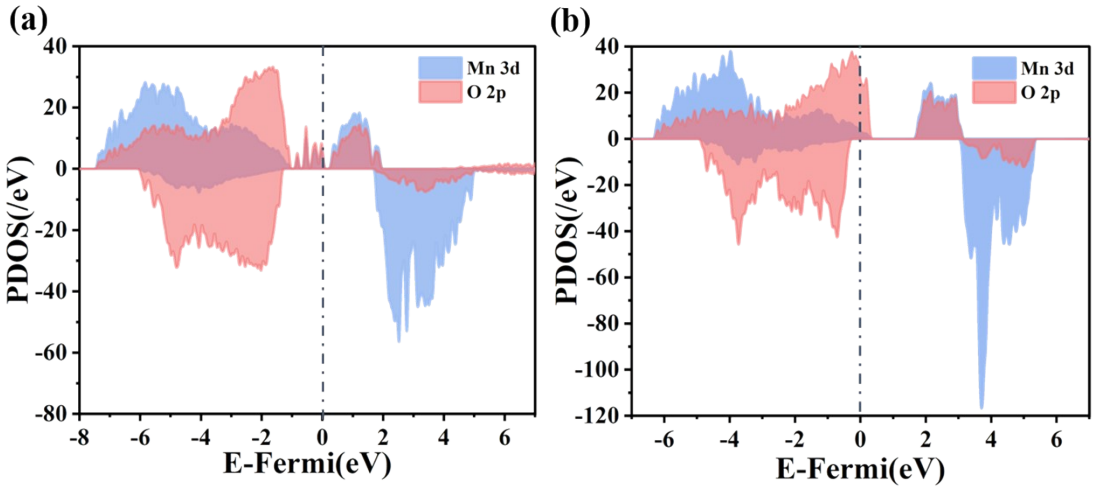

Figure S8. The pDOS of the Mn 3d and O 2p orbitals of $Na_xMg_{0.2}Mn_{0.8}O_2$ (x=0.7, 0.1). In the desodiation, the O 2p orbitals in the spin-up region move to higher energies and cross the Fermi energy level. This indicates the oxidation of O^{2-} to $O^{(2-n)-}$ upon desodiation.

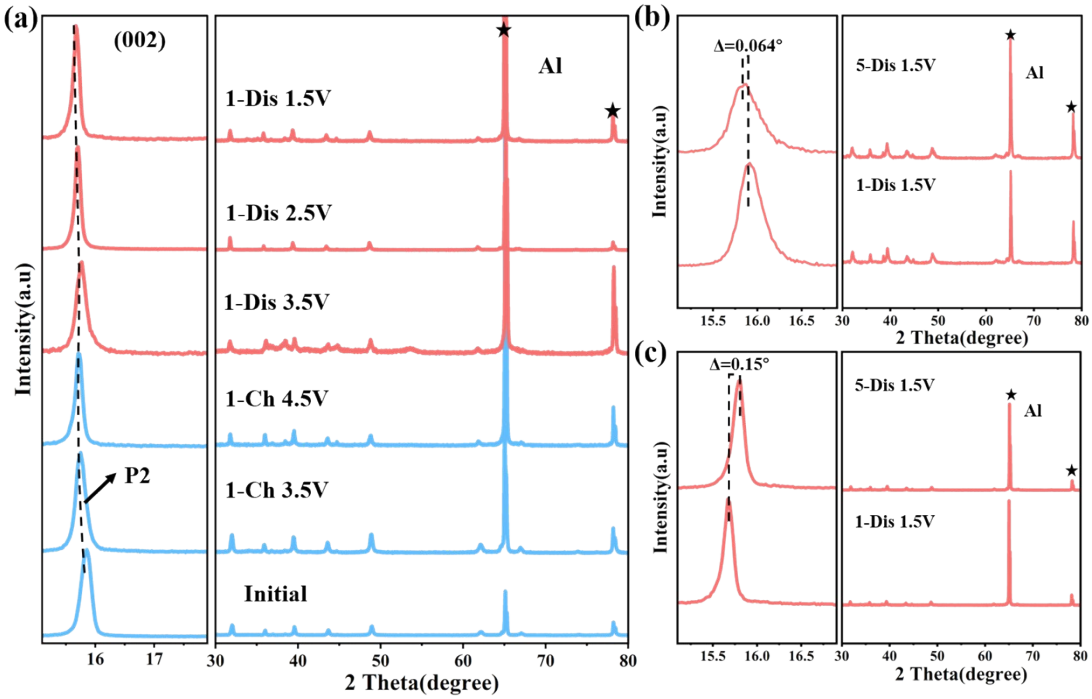

Figure S9. (a) Evolution of XRD patterns of P2-NMMO cathode during cycling. The change in the position of the main peaks (002) of NLMMO **(b)** and NMMO **(c)** can be observed from the XRD results at the end of the 1st and 5th discharges, and NLMMO was shifted by only 0.064°, while the NMMO was shifted by 0.15°.

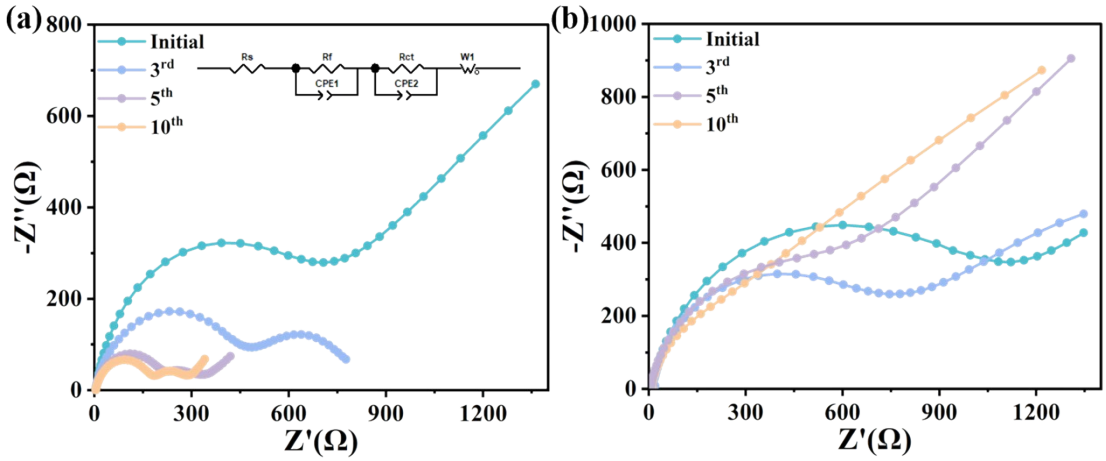

Figure S10. Impedance spectra of electrodes before cycling and after different cycles (Inset is the equivalent circuit). The fitting values of R_{ct} are listed in Table S4. Due to the formation of CEI during cycling, the impedance decreased and gradually stabilized in subsequent cycles. The resistance of the NLMMO was gradually reduced from 816 to 179.8 Ω, while the resistance of the NMMO was only reduced from 1203 to 607.8 Ω.

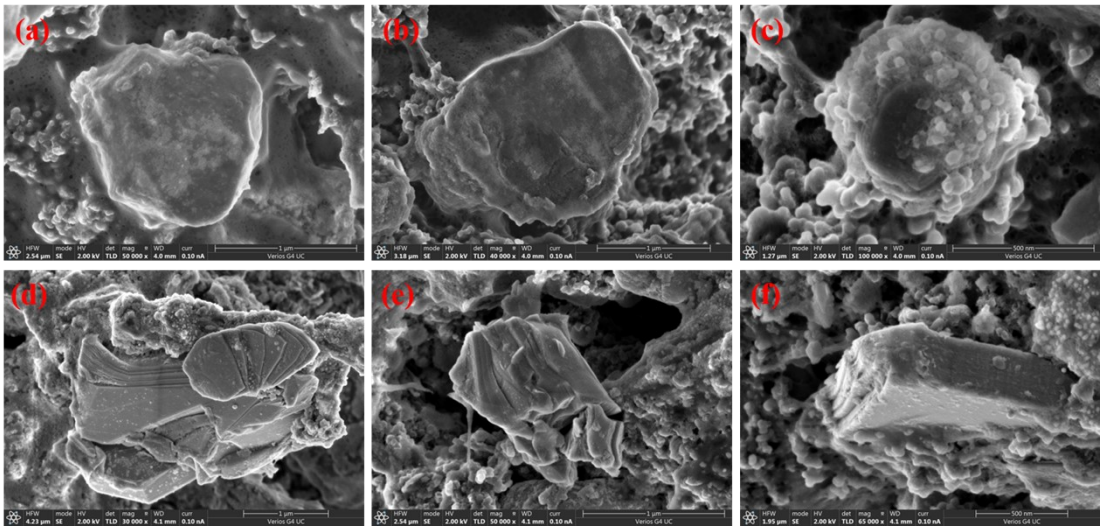

Figure S11. SEM images of NLMMO (a-c) and NMMO (d-f) after 10 cycles. The NLMMO still maintained the intact particles, while the NMMO showed a serious cracking. This increased the side reaction between NMMO and electrolyte, and also explained the decay phenomenon of its capacity.

Table S1. Lattice parameters of P2-NLMMO material derived from Rietveld refinement

atom	site	x	y	z	occ.
Nae	2d	0.66667	0.33333	0.25	0.43
Naf	2b	0	0	0.25	0.27
Li	2a	0	0	0	0.1
Mg	2a	0	0	0	0.2
Mn	2a	0	0	0	0.7
O	4f	0.66667	0.33333	0.08660	1

***P6₃/mmc*. a=b=2.88508 Å, c=11.08730 Å, Rp: 4.41 Rwp: 7.37 Rexp: 4 chi2: 2.62**

Table S2. ICP-OES results of P2-NLMMO and P2-NMMO materials

Sample	Measured atomic ration			
	Na	Li	Mg	Mn
NLMMO	0.69	0.11	0.2	0.71
NMMO	0.69		0.2	0.81

Table S3. Parameter table for button cell batteries

Materials	Cathodes' mass loading (mg)	Electrolyte amount (μl)	Radius (mm)	Thicknesses (μm)
NLMMO	**2.4784**	**150**	**14**	**20**
NMMO	**2.5504**	**150**	**14**	**20**

Table S4. The fitting values of R_{ct} for materials after different cycles

Materials	Initial	3rd	5th	10th
NLMMO	816	387.5	244.7	179.8
NMMO	1203	938.5	871.4	607.8

Table S5. Comparison of electrochemical performance (reversible capacity, capacity retention) with other ARR-involving layered sodium oxide cathodes

Materials	Operating voltage	Current Density	initial capacity	Capacity retention	Refs.
$Na_{0.65}Li_{0.22}Mn_{0.78}O_{1.99}F_{0.01}$	1.5-4.5	10 mA/g	177	87.8%	1
$Na_{0.66}Li_{0.22}Mn_{0.78}O_2$	1.5-4.5	10 mA/g	180	72%	1
$Na_{1.2}Mn_{0.4}Ir_{0.4}O_2$	1.5-4.4	0.1 C	137	72%	2
$Na_{0.8}Li_{0.27}Mn_{0.68}Ti_{0.05}O_2$	2-4.3	20 mA/g	143	78%	3
$Na_{2/3}Mn_{7/9}Zn_{2/9}O_2$	1.5-4.2	0.1 C	195	60%	4
$Na_{0.66}Li_{0.22}Mn_{0.775}Zr_{0.005}O_2$	1.5-4.5	0.05 C	197	81%	5
$Na_{0.75}Ca_{0.05}Li_{0.15}Fe_{0.2}Mn_{0.6}O_2$	1.5-4.5	0.1 C	208	42.3%	6
$Na_{2/3}[Zn_{1/9}Mn_{7/9}\square_{1/9}]O_2$	1.5-4.4	20 mA/g	204	63.41%	7
$Na_{0.67}Mg_{0.2}Mn_{0.8}O_2$	1.5-4.5	0.1 C	219.5	64.46%	8
$Na_{0.67}Zn_{0.2}Mn_{0.8}O_2$	1.5-4.5	0.1 C	208	64.9%	8
$Na_{0.73}Li_{0.11}Mg_{0.12}Mn_{0.77}O_2$	1.5-4.5	0.1 C	220	62%	9
$Na_{0.67}Ni_{0.2}Fe_{0.15}Mn_{0.65}O_2$	1.5-4.3	15 mA/g	207	31.4%	10
$Na_{0.7}Li_{0.1}Mg_{0.2}Mn_{0.7}O_2$	1.5-4.5	0.1C	217	84.3%	this work

Reference

1. Zhao, C.; Yang, Q.; Geng, F.; Li, C.; Zhang, N.; Ma, J.; Tong, W.; Hu, B., Restraining Oxygen Loss and Boosting Reversible Oxygen Redox in a P2-Type Oxide Cathode by Trace Anion Substitution. *ACS Applied Materials & Interfaces* **2021,** *13* (1), 360-369.
2. Zhang, X.; Qiao, Y.; Guo, S.; Jiang, K.; Xu, S.; Xu, H.; Wang, P.; He, P.; Zhou, H., Manganese-Based Na-Rich Materials Boost Anionic Redox in High-Performance Layered Cathodes for Sodium-Ion Batteries. *Advanced Materials* **2019,** *31* (27), 1807770.
3. Hu, B.; Geng, F.; Zhao, C.; Doumert, B.; Trébosc, J.; Lafon, O.; Li, C.; Shen, M.; Hu, B., Deciphering the Origin of High Electrochemical Performance in a Novel Ti-Substituted P2/O3 Biphasic Cathode for Sodium-Ion Batteries. *ACS Applied Materials & Interfaces* **2020,** *12* (37), 41485-41494.
4. Bai, X.; Sathiya, M.; Mendoza-Sánchez, B.; Iadecola, A.; Vergnet, J.; Dedryvère, R.; Saubanère, M.; Abakumov, A. M.; Rozier, P.; Tarascon, J.-M., Anionic Redox Activity in a Newly Zn-Doped Sodium Layered Oxide P2-Na2/3Mn1−yZnyO2 (0 < y < 0.23). *Advanced Energy Materials* **2018,** *8* (32), 1802379.
5. Zhao, C.; Li, C.; Yang, Q.; Qiu, Q.; Tong, W.; Zheng, S.; Ma, J.; Shen, M.; Hu, B., Anionic redox reaction in Na-deficient layered oxide cathodes: Role of Sn/Zr substituents and in-depth local structural transformation revealed by solid-state NMR. *Energy Storage Materials* **2021,** *39*, 60-69.
6. Wang, Y.; Zhao, X.; Jin, J.; Shen, Q.; Zhang, N.; Qu, X.; Liu, Y.; Jiao, L., Low-cost layered oxide cathode involving cationic and anionic redox with a complete solid-solution sodium-storage behavior. *Energy Storage Materials* **2022,** *47*, 44-50.
7. Yang, L.; Liu, Z.; Shen, X.; Li, S.; Hu, Z.; Kong, Q.; Ma, J.; Li, J.; Lin, H.-J.; Chen, C.-T.; Chen, J.-M.; Haw, S.-C.; Wang, X.; Yu, R.; Wang, Z.; Chen, L., Effect of vacancy-tailored Mn3+ spinning on enhancing structural stability. *Energy Storage Materials* **2022,** *44*, 231-238.
8. Ji, H.; Ji, W.; Xue, H.; Chen, G.; Qi, R.; Huang, Z.; Fang, H.; Chu, M.; Liu, L.; Ma, Z.; Xu, S.; Zhai, J.; Zeng, W.; Schulz, C.; Wong, D.; Chen, H.; Xu, J.; Yin, W.; Pan, F.; Xiao, Y., Synergistic activation of anionic redox via cosubstitution to construct high-capacity layered oxide cathode materials for sodium-ion batteries. *Science Bulletin* **2023,** *68* (1), 65-76.
9. Liu, J.; Qi, R.; Zuo, C.; Lin, C.; Zhao, W.; Yang, N.; Li, J.; Lu, J.; Chen, X.; Qiu, J.; Chu, M.; Zhang, M.; Dong, C.; Xiao, Y.; Chen, H.; Pan, F., Inherent inhibition of oxygen loss by regulating superstructural motifs in anionic redox cathodes. *Nano Energy* **2021,** *88*, 106252.
10. Wang, Y.; Hu, G.; Peng, Z.; Cao, Y.; Lai, X.; Qi, X.; Gan, Z.; Li, W.; Luo, Z.; Du, K., Influence of Li substitution on the structure and electrochemical performance of P2-type Na0.67Ni0.2Fe0.15Mn0.65O2 cathode materials for sodium ion batteries. *Journal of Power Sources* **2018,** *396*, 639-647.